Computational Modelling of Wing Downwash Profile with Reynolds-Averaged and Delayed Detached-Eddy Simulations

K. J. Benjamin Tan[1]
University of Glasgow Singapore, Singapore 139661

P. C. Wang[2]
Singapore Institute of Technology, Singapore 138683

and

S. Srigrarom[3]
University of Glasgow Singapore, Singapore 139661

This paper describes the computational model to predict downwash for a conventional fixed wing configuration at flight scales ($Re_{MAC} = 2.26 \times 10^7$). The lack of resolution in the downwash wake region resulted in an over-dissipation of the turbulent behaviour of airflow in the wing's wake. This artificially inflates the effectiveness of the horizontal stabilizer where an over-prediction of pitch stiffness was observed. To resolve this over-dissipation, both the Reynolds-Averaged and Delayed Detached-Eddy Simulation methodology were adopted to accurately capture the downwash profile leaving the wing. Comparisons between the estimation of wall shear stresses and viscous wall unit against a 'first-cut' simulation are made and discussed. Fundamental features of the downwash profile including the spatial and temporal scales used for the mesh are also presented and detailed in this paper.

Nomenclature

C	=	Courant number
C_f	=	coefficient of friction
f_d	=	blending factor
$\tilde{S}$	=	source term
τ_w	=	wall shear stress
u	=	component of velocity parallel to wall
U_z	=	vertical velocity component
μ	=	dynamic viscosity
μ_t	=	turbulent viscosity
$\tilde{\nu}$	=	modified turbulent viscosity
Δ	=	subgrid length scale
Δt	=	time step
ε	=	downwash angle
α	=	angle of attack

All other symbols have their usual meaning and positive convention follows the aircraft principal axes (front, right, down) with the origin at wing leading edge.

---

[1] Postgraduate Research Student, University of Glasgow Singapore, Singapore 139661, AIAA Student Member.
[2] Assistant Professor, Engineering Cluster, Singapore Institute of Technology, Singapore 138683.
[3] Associate Professor, Aerospace Systems, University of Glasgow Singapore, Singapore 139661, AIAA Member.

I. Introduction

Longitudinal stability is the most important flight characteristic of an aircraft where prior to any flights, its stability must be ascertained.[1] As the horizontal stabilizer for a conventional fixed wing configuration is the dominant contributor to pitch stability, the assessment of its effectiveness and local airflow is crucial.[2] When the tail lies within the wake of the wings, the impingement of airflow from the wing's wake alters the tail's performance. The effectiveness of the horizontal stabilizers in this situation can be theoretically treated by introducing a tail efficiency factor where a ratio between the freestream and local horizontal tail dynamic pressures is taken.[2] Typical values are 0.8 to 1.2.[3] This downward deflection of airflow alters the effective angle of attack for the horizontal stabilizer which affects the amount of force and moments generated by the tail for pitch. If the vertical component(s) of this field can be numerically captured, the downwash angle can be estimated. This effect of downwash on the tail is significant and must not be neglected. Having the effective angle of attack at the tail altered subsequently affects the aircraft's trim. These interactions can only be assessed by use of simulations or experiments.[4]
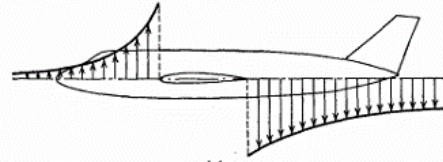

Figure 1. Qualitative pattern of up and downwash induced by wing vorticity.[2]

From past preliminary studies on aerodynamic data acquisition,[5] an over-prediction was observed for pitching moment coefficients C_M across angles of attack, represented by a steeper C_{M_α} in comparison with published wind tunnel data.[6] This over-prediction of the pitch stiffness was attributed to the lack of resolution in the region of wing downwash, which in a conventional fixed wing configuration, would affect the modelled effectiveness of the horizontal stabilizer. The lack of foresight to capture these fore-aft aerodynamic interactions with sufficiently fine mesh led to numerical dissipation of turbulent properties of the airflow. The motivation and importance of capturing results in this region branches from the observations made from these preliminary past work.[5]

For a finite wing, the two prominent flow features are the wing tip vortices and vortex sheet.[7] Emphasis here is placed on the downwash along the vortex sheet. This wake has been the subject of study by experimental methods and formulated to predict downwash angles and wake characteristics.[8,9] The formulated results from these work show that the wake exhibits different characteristics along the span-wise direction of the wing being studied and for practical purposes, the mutual interference between the fuselage and wing or tail has to be considered.

A focused geometry shown in Fig. 2 is used by exclusively modelling the plain wing and tail. This was first explored from the approximation that lift for the wing-body combination can be represented by only the wings but inclusive of the midsection masked by the fuselage.[5,10] This same principle is applied to the horizontal stabilizers which are analogous to the wings but where their contribution are towards stability. However, the presence of the midsection of the horizontal stabilizers that was initially masked by the fuselage are also modelled. The benefit of such a simplified model in addition to exploiting symmetry, is that it can make the entire meshing and simulation process much more economical, especially when the flow conditions are at flight Reynolds numbers. This range of airspeed is observed for the actual aircraft that the geometry here is modelled after (0.19 < M < 0.45).[11,12] The wind tunnel data that is used for validation here was also corrected for these freestream velocities (M = 0.23).[6]

The absence of the fuselage has a considerable impact on the stability and aerodynamics of the geometry as a fuselage typically shifts the aerodynamic centre aft, thus a Wing-Tail geometry is likely to be longitudinally stiffer than a Wing-Body-Tail configuration.[13] In the context of a wing-tail only configuration, this makes the choice of location to be studied challenging as computationally modelling of such comprehensive datasets[9] would be exhaustive. Furthermore, results involving the midspan (along aircraft symmetry plane) are likely to be interfered by a fuselage. Hence, results for the downwash are taken at a wing outboard station of 20% wing span (which corresponds to approximately 25% tail span) from the aircraft centerline.

The studies on downwash and wake behind airfoils have indicated that empirical methods are sufficient for use as a basis for downwash computation and wing tip vortices may be neglected for the purposes of downwash studies.[8] Importantly, the vertical displacement of the vortex sheet due to downflow must be taken into consideration for calculations. This vertical velocity is quantified in the following studies.[9] A characteristic pattern of the up and downwash of vertical velocity components along the longitudinal direction around the wing is shown in Fig. 1. The vertical quantities of velocity are critical in estimating downwash angles based on the freestream. Resolving for flow fields trailing from the wings and how the physical presence of the tail affects this characteristic downwash profile are the focus, and require refinements to the mesh to capture these features. These are in the form of a mesh sensitivity test.

A brief assessment of the wing tip vortex size is also done to determine the profile of vortex tangential velocities towards the tail. At this short distance, it is very likely that the vortex is still developing and shows that the wing tip

vortex has little effect on the tail as these velocities diminish exponentially.[14,15] This can also be observed with the Biot-Savart law[7] relating the tangential velocity to a point at distance r from the vortex filament:

$$d\vec{V} = \frac{\Gamma}{4\pi} \frac{\overrightarrow{dl} \times \vec{r}}{|r^3|}$$

(1)

The balance between theory, experimental, and computational methods have been thoroughly discussed.[16,17] Unlike physical approach such as flight testing and wind tunnel experiments, CFD (Computational Fluid Dynamics) provides visualisation of the flow field and quantifying of flow variables at discrete points without interference from necessary probes and supports used in experiments.[4] Theoretical methods under ideal assumptions do not give insight to prediction of the flow field properties involved, especially the development of the downwash, which is likely to be turbulent and unsteady. Misrepresentation of the flow characteristics in such regions can lead to unforeseen and undesirable aircraft behavior that can compromise safety and affect the design and production of aircraft.[18] The need for advances in applying novel CFD modelling methods to enhance the understanding of aerodynamic interactions motivates this research.[19,20]

The following work will first present the methods used for the purposes of this study. Analyses are conducted first with the more economical RANS (Reynolds Averaged Navier Stokes) methods for turbulence modelling with the Spalart-Allmaras one-equation turbulence model. Then, a more advanced model, DES (Detached Eddy Simulations) that employs a hybrid RANS/LES (Large Eddy Simulations) modelling technique is used.[21] Conceptually, DES treats the near-wall with RANS formulations whereas regions farther are treated with LES. This reduces computational, but not necessarily grid[22] requirements, especially near the walls but simultaneously allows LES-like modelling for regions further from the walls.[23] As flight scales are simulated, computational requirements are steep, thus refinements near the wall are of less focus as compared to the downwash region of interest. Solving for the fluctuating variables require exorbitant levels of computational power such as DNS (Direct Numerical Simulation), and therefore DES or LES would likely prevail to be better suited for this work.[24]

Wall modelling for the initial RANS method where calculation of the wall shear stress for determining the normalized wall unit is compared with a 'first-cut' simulation are also discussed. Spatial and temporal resolutions that are used for the chosen modelling techniques are also presented. This includes mesh sensitivities studies for the vertical downwash velocity component over three refinements of cell edge lengths. The observed qualitative patterns of downwash are then quantified and normalised by the peak velocities and wing mean aerodynamic chord, C_{MAC}. This pattern is also presented with and without the horizontal stabilizer. Steady-state results are presented after convergence, which determined by monitoring for unchanging values of aerodynamic coefficients and the vertical velocity component in the downwash region. Temporal results are time-averaged after developed flows are obtained with statistically-steady states.

II. Methodology

A. Geometry

The geometry is modelled after a C-130H with an aspect ratio of 10.09, a wing and tail span of 40 m and 16 m, respectively. It has a mean aerodynamic chord, C_{MAC} of 4.18 m. The tail is located approximately 8.7 m ($3.5C_{MAC}$) aft of the wing leading edge.[25] All angles of attack and incidence are taken with reference to the freestream and the fuselage reference line. The wing comprises of the NACA 64A318 at the root with a 3 ° angle of incidence, and the NACA 64A412 at the tip with an angle of incidence of 0 ° (3 ° wing washout). The horizontal stabilisers are an inverted NACA 23015 with an angle of incidence of -1.75 °. Geometries are worked on in the order of increasing complexity, resulting 4 different geometries:

1. 2D Wing   (2D-W)
2. 2D Wing+Tail   (2D-WT)
3. 3D Wing   (3D-W)
4. 3D Wing+Tail   (3D-WT)

The 2D geometry chords lengths are modelled after the wing MAC the average tail chord for the horizontal stabilizers. The 2D geometries serve as the initial validation models for CAD accuracy and were found to be in good agreement compared to the experimental reports.
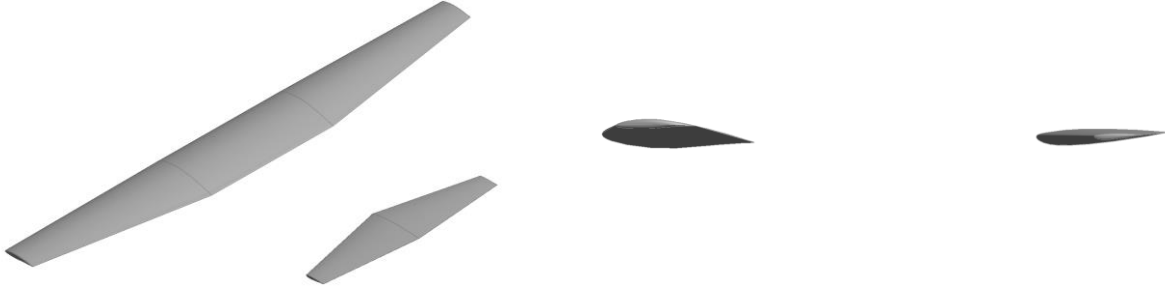
Figure 2. Isometric and side view of the 3D-WT geometry

B. Numerical Methodology

Closure for the incompressible Reynolds-Averaged Navier-Stokes equations are modelled by the Spalart-Allmaras model,[26] which uses a one-equation transport to solve for a modified turbulent viscosity $\tilde{v}$, implemented *without* the trip term f_{t2}:[27]

$$\frac{\partial \tilde{v}}{\partial t} + u_j \frac{\partial \tilde{v}}{\partial x_j} = c_{b1}\tilde{S}\tilde{v} - c_{w1}f_w\left(\frac{\tilde{v}}{d}\right)^2 + \frac{1}{\sigma}\left[\frac{\partial}{\partial x_j}\left((v + \tilde{v})\frac{\partial \tilde{v}}{\partial x_j}\right) + c_{b2}\frac{\partial \tilde{v}}{\partial x_i}\frac{\partial \tilde{v}}{\partial x_i}\right] \tag{2}$$

Where the source term $\tilde{S}$ is implemented with the f_{v3} term:[28]

$$\tilde{S} = f_{v3}\Omega + \frac{\tilde{v}}{k^2 d^2}f_{v2} \; ; \; f_{v3} = \frac{(1 + xf_{v1})(1 - f_{v2})}{x} \tag{3}$$

The turbulent viscosity μ_t is then computed for the Boussinesq assumption for the Reynolds stress tensor:

$$\mu_t = \tilde{v}f_{v1} \tag{4}$$

The model constants are applied as recommended.[26,29]

The DDES model is achieved by altering the length scale d in the destruction term (Eq. 2):[22]

$$\tilde{d} = d - f_d max[0, d - C_{DES}\Delta] \tag{5}$$

Where $C_{DES} = 0.65$. The blending factor f_d distinguishes between the boundary layer and freestream where $f_d = 0$ returns a RANS solution while $f_d = 1$ brings a length scale Δ, which is determined by:

$$\Delta = (\Delta x \Delta y \Delta z)^{\frac{1}{3}} \tag{6}$$

The SIMPLE and PISO solution algorithms are used for pressure-velocity coupling for the steady (RANS) and transient (DDES) solutions, respectively.[30] Transient results would also give insight on any fluctuations present in the flow field.

Preliminary parametric studies on the wing root section showed that both 2nd order upwind and 3rd order MUSCL discretisation schemes with the one- and two-equation eddy-viscosity turbulence models (Spalart-Allmaras (SA) and compared with the Realisable k-ε, both treated with standard wall functions) provide results which are equally good and in agreement with the available wind tunnel data[6] for prediction lift, but with a slight over-prediction for drag and pitch,[5] as seen in Fig. 5.

C. Spatial (Mesh) and Temporal Resolution

Empirical methods for calculation of the viscous wall unit (y+) are verified against a 'first-cut' simulation. All simulations were attempted at flight conditions (M = 0.23, $Re_{MAC} = 2.26 \times 10^7$) and validated against available wind tunnel data.[6] Given the experimental setup is ambiguous, the assumption of standard sea-level conditions ($\rho_\infty = 1.225$ kg/m^{3}) are taken. Modelling of the geometry also excludes any possible experimental supports or probes, which interferes with measured results.[31]

The wall shear stress τ_w within the inner region dominates the flow characteristics.[32] The wall grid spacing is determined empirically by friction velocity and the coefficient of friction for estimating wall shear stress with flow Reynolds Numbers > 10^9:[33]

$$\tau_w = \frac{1}{2} \rho V^2 C_f \tag{7}$$

Where;

$$C_f = [2 \log_{10}(Re) - 0.65]^{-2.3} \tag{8}$$

This method for first-cell height estimation is then validated at against a 'first-cut' simulation with the y+ measured and averaged at increments of 0.25c across the aerofoil upper surface. This is found to be in good agreement (average y+ 4% smaller) with the wall shear stress relation for Newtonian fluids:[32]

$$\tau_w = \mu \left(\frac{\partial u}{\partial y}\right)_{y=0} \tag{9}$$

Cases are then discretised with a body fitted grid of y+ = 30 at a growth rate of 1.2 up to 15 layers. Mesh sensitivity study is conducted by halving the element edge lengths in the mesh refinement region encompassing the wing and tail. Convergence is determined by observing for unchanging aerodynamic coefficients and vertical velocity component U_z. Halving the edge length in the refinement region results in a greatest of 2% change of U_z that is measured just forward of the horizontal stabilizer at 25% tail span.

Elements in the refinement are almost cubic with a maximum cell aspect ratio of 1.09. The edge lengths in Table 1 are presented as an average and further expressed as a percentage of C_{MAC}.

The refinement zones for the mesh for the Fine case exceeded mesh counts and was unlikely to have brought significant gains. To utilize the Fine mesh for the time dependent case, the refinement regions were resized to refine 9 m span-wise from the wing root and extending downstream to encompass the entire horizontal stabilizer. This resizing was made after determining that the developing tip vortices has a negligible impact on the downwash for such a high wing aspect ratio. The Fine mesh is used for all cases.

Table 1. Mesh sensitivity of vertical velocity U_z

	Avg. cell edge length (% MAC)	Peak U_z 3D-W	Peak U_z 3D-WT
Coarse	0.0746 m 1.79 %	3.43 m/s	5.01 m/s
Medium	0.0377 m 0.9 %	3.45 m/s	4.91 m/s
Fine	0.019 m 0.45%	3.49 m/s	-

Temporal scales are determined with the Courant-Friedrichs-Lewy condition:[34]

$$C = \frac{U_\infty \Delta t}{\Delta x} \leq C_{max} \tag{10}$$

Where the edge length Δx is taken from cubic elements in the refinement regions. A time step Δt of 1e-4 s produces a Courant number of 0.41. The flow is given 1 s to develop which at this speed corresponds to approximately flow past 5 times the downwash domain length. This allows the flow to develop into a statistically steady state before sampling for time averaged results.
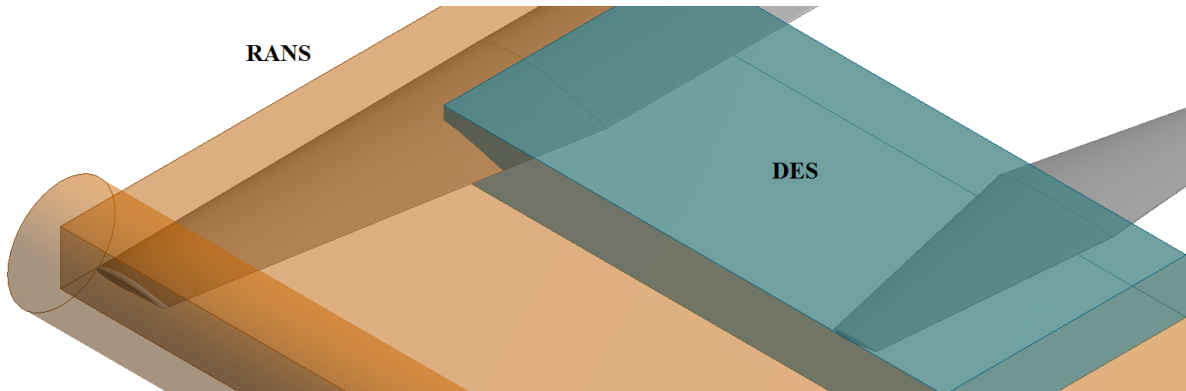

Figure 3. Illustration of grid refinement bounds for RANS (larger - orange) and DDES (zonal - blue).
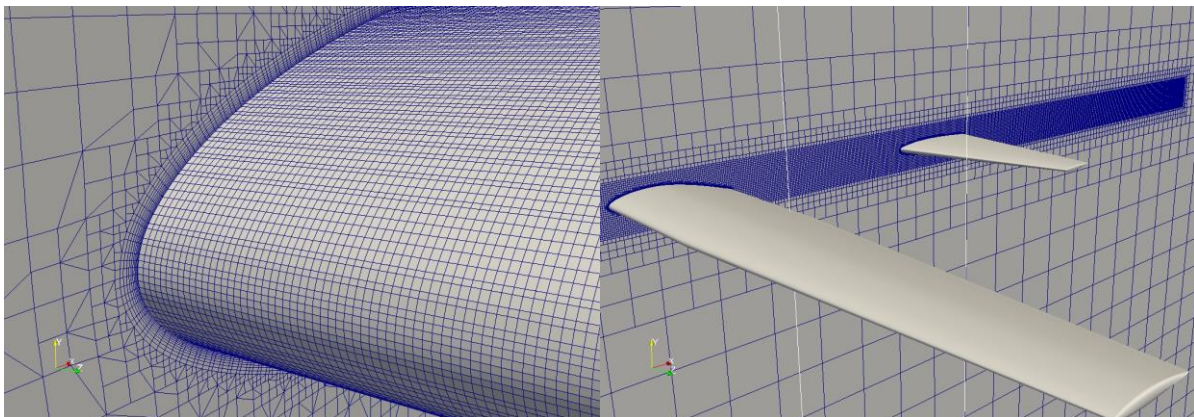

Figure 4. Body fitted grid [left] and refinement [right]. Results for downwash U_z taken along vertical white lines at every 1m increment from wing trailing edge to tail leading edge, 20% wing span from symmetry plane.

III. Results and Discussion

The following are the results that compare the accuracy of the 1st & 2nd order Upwind, and 3rd order MUSCL discretization schemes against the published wind tunnel data for the wing root section (NACA 64A318). It is determined that the 2nd and 3rd order schemes are equally accurate and only the most accurate results are shown in Fig. 5 for clarity.
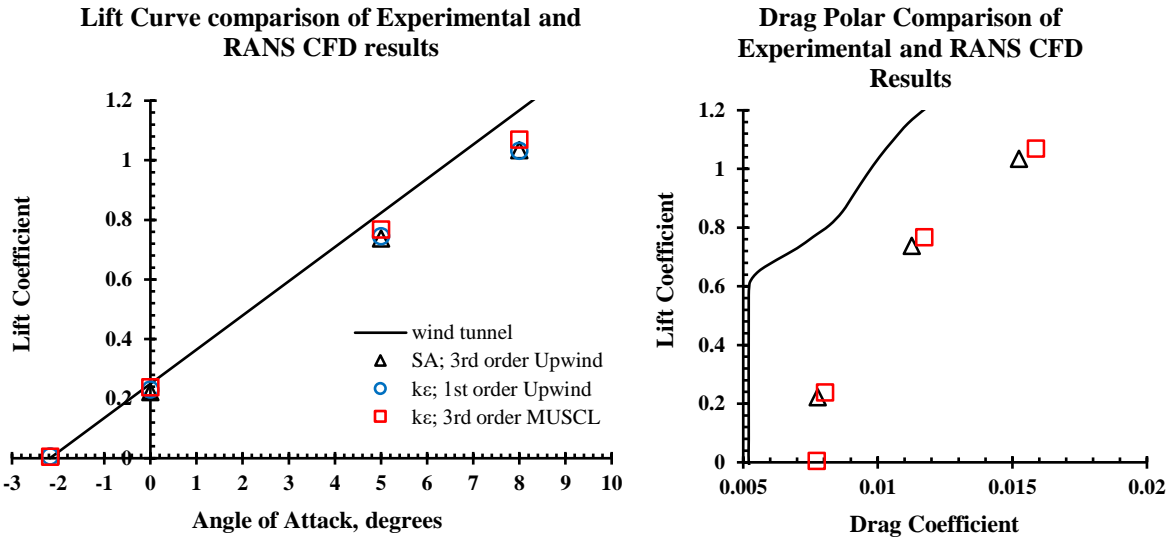

Figure 5. Validating the accuracy of discretization schemes for lift coefficient and drag polar against experimental results for the wing root (NACA 64A318). Axes are truncated to focus on numerical results.
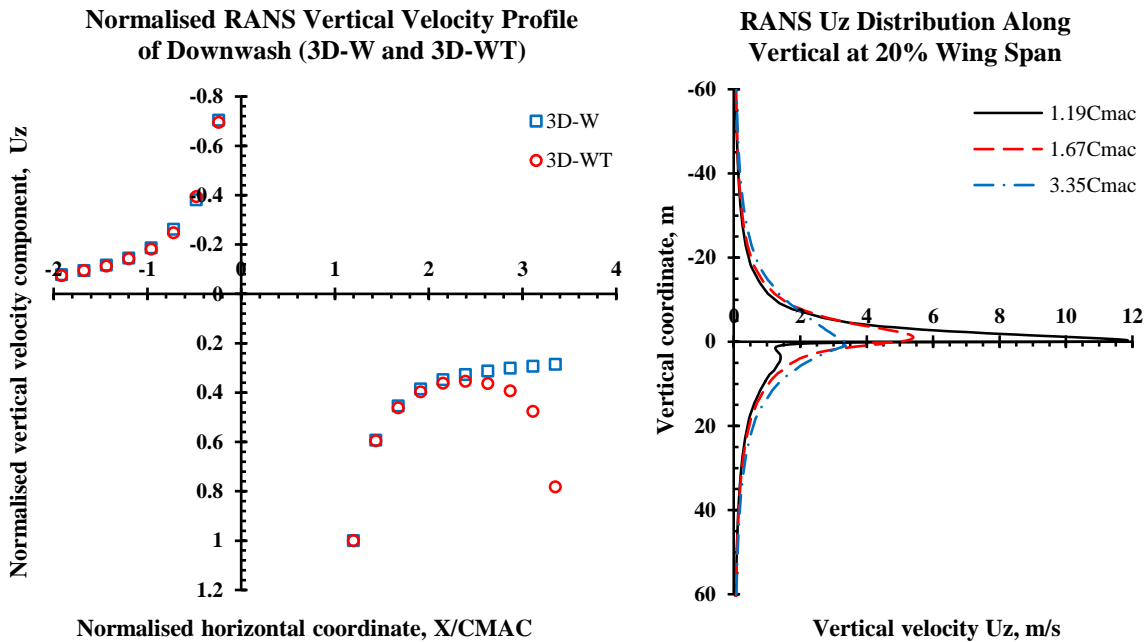

Figure 6. [Left] Pattern of up and downwash profile for the 3D-W and 3D-WT geometries. [Right] Distribution of U_Z along vertical at $1.19C_{MAC}$ (aft of wing), and $3.35C_{MAC}$ (fore of tail).

The refinement region used for the RANS simulations are box shaped as shown in Fig. 3, and a cylinder along the length of the wing tip vortex filament. This allows capturing of the developing tip vortices and subsequently give solutions on the tangential velocities involved and their potential impact on the downwash closer to the root.

Results for the computationally modelled up and downwash pattern as well as distribution of downwash are presented in Fig. 6. Although the peak velocities are portrayed to be with reference to the same arbitrary horizontal datum, inspection of these results show that they occur at different elevations. The data are taken at discrete points spaced 0.06 m vertically apart and from this, the maximum horizontal height difference between the highest and lowest vertical velocities to be 0.0972 m. Relative to the maximum U_z observed at $1.2C_{MAC}$ to be 11.86 m/s, this difference in elevation is small. A greater magnitude of downwash can be observed towards the horizontal stabilizer leading edge for the 3D-WT geometry that is induced by the tail leading edge vorticity. It can also be observed from the distribution of U_z along the vertical that the downwash components diminish exponentially (Fig. 6, right). The dissipation of these velocities are at approximately the span of the aircraft (40 m). However, the mesh in these far-field regions are without any refinements as seen in Fig. 4.

The angle which the local airflow impedes on the tail alters the local and effective angle of attack on the horizontal stabilizer. This downwash angle ε, is estimated as a function of angle of attack α, to be:[3]

$$\frac{d\varepsilon}{d\alpha} = \frac{2C_{L_\alpha}}{\pi AR} \tag{11}$$

Where C_{L_α} and AR is the lift-curve slope in radians and aspect ratio of the *wing*, respectively. With the fuselage reference line levelled, the wings are at 3 ° angle of incidence, giving $C_{L_\alpha} = 0.528\ rad^{-1}$, neglecting stall angles.[6] This returns $d\varepsilon/d\alpha = 0.333$. Taking the component of U_z just fore of the horizontal stabilizer with respect to the freestream, the downwash at this angle of attack can be calculated to be 2.46 °.
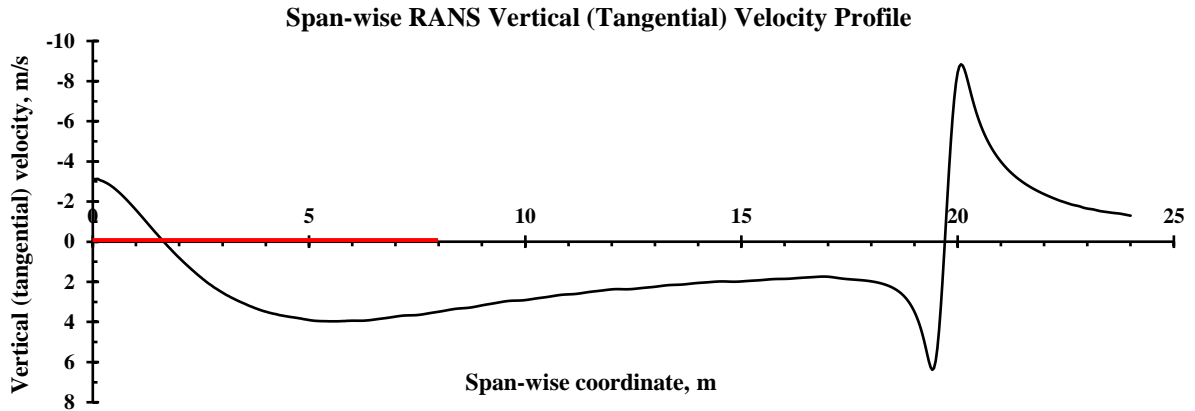

Figure 7. (Semi) Span-wise velocity profile and across wing tip vortex core, just fore of horizontal stabilizer. Red line depicts horizontal tail semi span.

In Fig. 7, the span-wise vertical velocity profile is shown at just fore of the horizontal stabilizer (red line depicts horizontal tail semi-span), plotted across the wing tip vortex core. It can be observed that velocities diminish exponentially beyond the core radius at < 18 m wing span. These velocities diminish at the mid-span due to the wing's large aspect ratio. This helps determine that the vertical tangential velocities has a negligible impact on the downwash region towards the tail. The change in values observed towards the root are caused by the deflection of airflow around the leading edge of the stabilizer. The midsection of the tail is supposed to be masked by the fuselage/empennage section but however, is modelled here.

The vortex core radius measured at $3.35C_{MAC}$ (plane at tail leading edge) is in agreement with typical values,[14] where the radii, defined as the distance from the vortex core to the point of maximum tangential velocity is in the order of 1% wing span (Fig. 9). The characteristic tangential velocity profile is also observed. However, when comparing the results to three *idealized* models of *trailing* wake vortices,[15] results differ. The estimation of the vortex strength by initial circulation Γ_0, for the calculation of tangential velocities with the idealized models is given by:

$$\Gamma_0 = \frac{Mg}{\frac{\pi}{4}\rho b U_\infty}$$

(12)

Where Mg is the weight of the aircraft. However, this is best approximated with the aircraft in equilibrium, and the results under which the conditions are taken may not be in cruise although flight Reynolds numbers are simulated.[35] The vortex core size from the results here are very likely to be still developing, as they are taken along the plane in the downwash regions. It can be seen in Fig. 8 that the vortex core diameter is small - but with high intensity by judging from the tangential velocities in Fig. 7 - relative to the span of downwash.
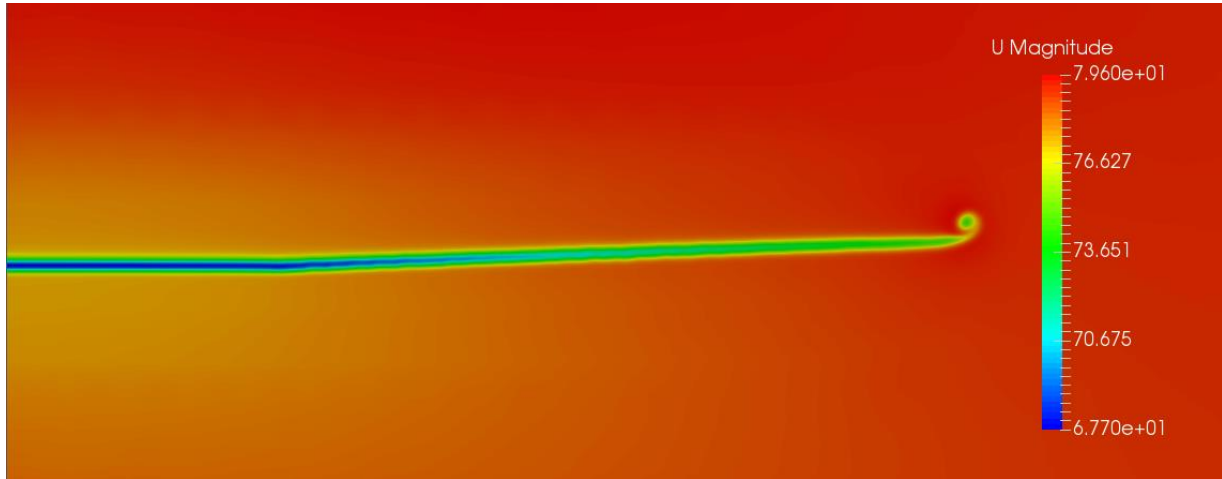

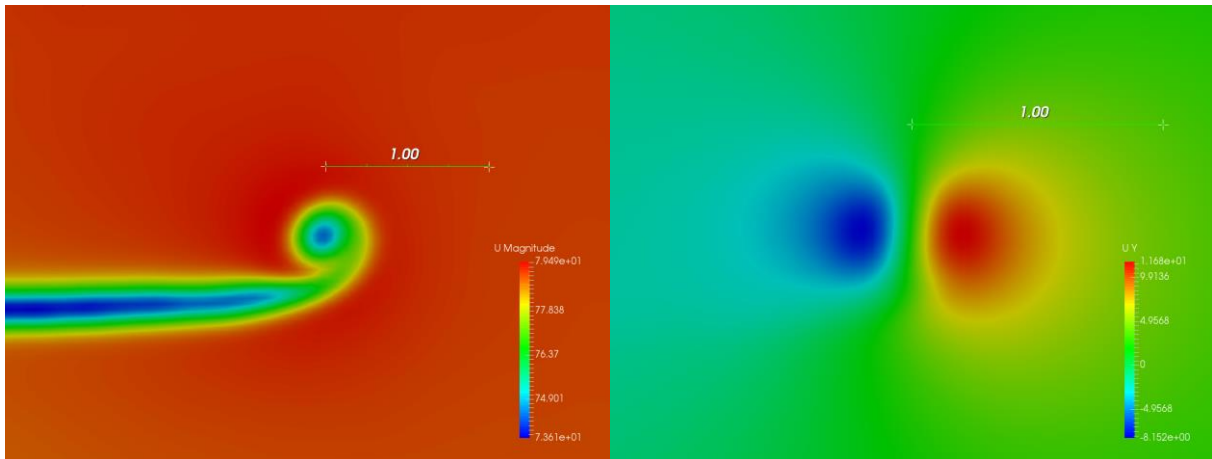**Figure 8. Span-wise velocity magnitude contour along plane at 1.6C$_{MAC}$**

Figure 9. [Left] Close-up of wingtip vortex. [Right] Vertical velocity U$_Z$ contour. Embedded scale depicts 1.00 m.

As RANS solutions are able to only resolve for the mean variables of the flow field by Reynolds decomposition, transient analyses are required to provide further insight to this profile and on any unsteadiness to these results. These datasets are time-averaged to provide their mean and fluctuating values - represented as a standard deviations - of velocities across the same sampled locations used in RANS. Only the 3D-WT model and mesh was used for the transient case.

DDES solutions are conducted at the inboard section of the wing root only (Fig. 3). For these analyses, the flow referencing the freestream, is given 1 s to develop. This corresponds to approximately 5 times the flow past the chord-wise domain length encompassing the wing and tail. After which, data are sampled between 1 < t < 1.5 s, and saved

at every 50 time steps where Δt =1e-4 s and time-averaged. This amounts to 5000 time samples. Within the initial 0.1 s, an initial vortex roll up[36] can be observed trailing the wings (Fig. 11).

There is an average standard deviation of 0.561 m/s in peak U_z across the sampled data (Fig. 10). The greatest fluctuations occur near the trailing and leading edges of the wing and tail. Similar to the RANS solution, the flow can be seen to be developed, with relatively consistent deviation in U_z, past $2C_{MAC}$ before being affected by the horizontal stabilizer indicated by a further downward deflection by increase of U_z. These fluctuations show that the effective angle of attack met at the tail leading edge is also subject to fluctuations. Taking these limits into consideration, the time-averaged effective range of downwash angle ε can be again determined by the component of U_z against the freestream, to be 2.84 ± 0.27 °. This is effectively a ± 10% variation in the downwash angle.

DDES Time Averaged Vertical Velocity Profile of Downwash (3D-WT)
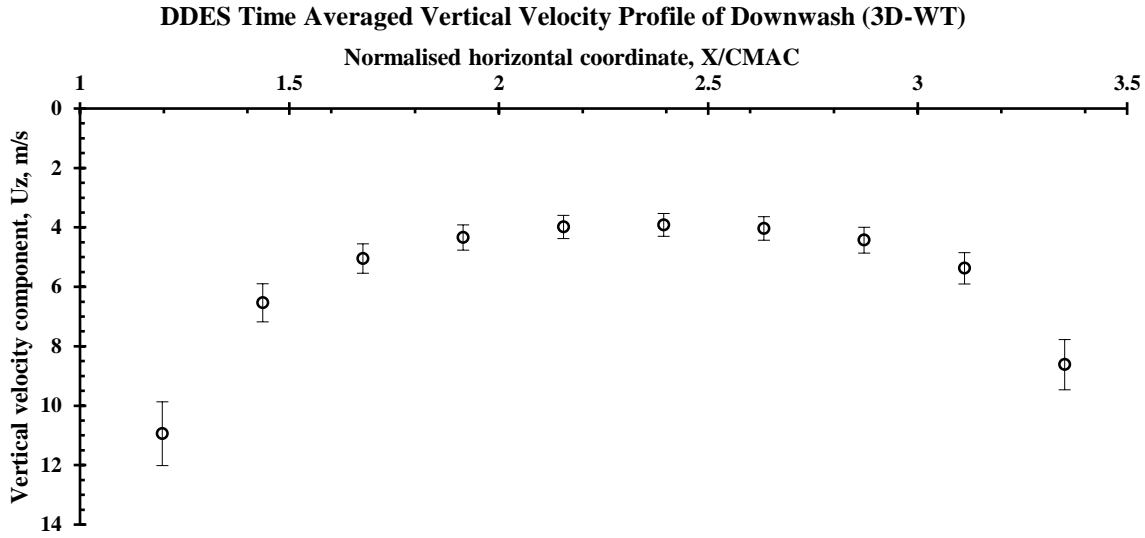

Figure 10.   Pattern of time averaged (1 < t < 1.5) downwash for the 3D-WT geometry. Error bars denote the standard deviation for peak U_z.

The downwash angle calculated from the RANS simulation results using the vertical velocity component U_z are similar and in agreement to be within the standard deviation observed by the DDES time-averaged results (Table 2). These downwash angles are supported by values obtained in the available experimental results and charts with an expected under-prediction of approximately 2-3 °.[8-9] It must be considered that the experimental results were conducted with a lift coefficient of 1.0. For the geometry used in this work, the wings generate a lift coefficient of approximately 0.3 at this designed angle of incidence. As the downwash angle is a function of wing lift coefficient, it is arguable that the results obtained here are relatively accurate. The available data also considers wing aspect ratios and possible flaps.

The results for the time-averaged DDES-resolved downwash profile agree thoroughly with the RANS solution, with the RANS results across the profile averaging at 1.4% error from DDES. Although the purpose of obtaining the characteristic profile could be accomplished economically by RANS, a time dependent solution provides insight on the fluctuation of velocities across the profile, as shown in Fig. 10, and on other flow features such as the starting vortex due to circulation (Fig. 11), which cannot be obtained via RANS.

Computational challenges were faced for DDES because of simulation of the fully scaled geometry at flight Reynolds numbers. These demanding requirements have been highlighted[19,21] and the DDES case here utilizes 90 million elements with just the refinement box

Table 2.   Numerical comparison of peak U_z time-averaged DDES and RANS result (C_{MAC} = 4.178 m)

X (m)	Peak U_z (m/s)		
	DDES	RANS	% Diff.
5	10.89	10.94	0.50
6	6.49	6.54	0.76
7	5.04	5.05	0.21
8	4.32	4.34	0.42
9	3.95	3.99	0.83
10	3.87	3.92	1.23
11	3.96	4.04	1.94
12	4.29	4.43	3.30
13	5.19	5.38	3.60
14	8.52	8.62	1.16
Avg.	-	-	*1.40*

10

capturing *part* of the downwash. At these spatial and temporal scales, approximately 9 days of computational time and 1 TB of data are used just for the transient case.

The meshing techniques used can be improved. Having a box-shaped enclosure to define mesh refinement as seen in Fig. 4 unnecessarily inflates the amount of elements in regions unrequired to capture the thin vortex sheet trailing the wings, especially at such a benign angle of attack. By optimizing the mesh, the turbulent scales involved could have been better resolved.
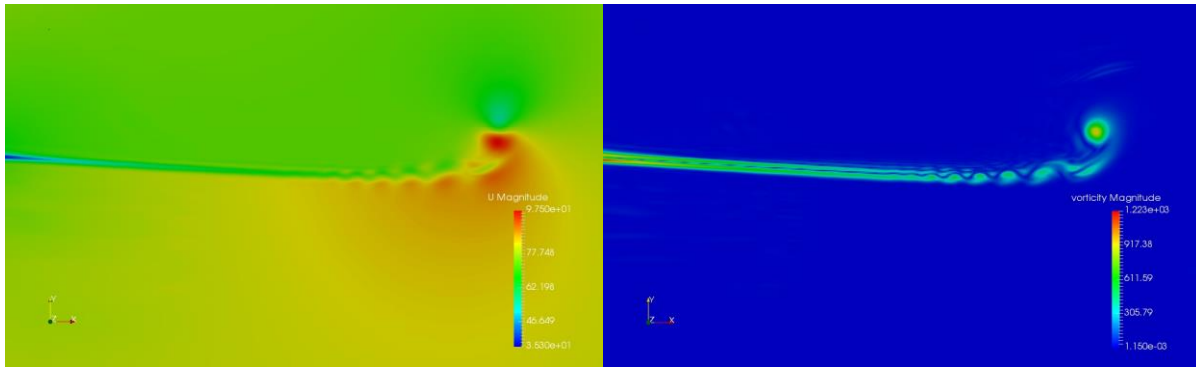

Figure 11.   Instantaneous chord-wise velocity magnitude and vorticity contours of starting vortex rollup leaving the wing at t = 0.05 s. Peak contours show velocity = 97.5 m/s and vorticity = 1223 s⁻¹

IV. Outlook

While validating the geometry against experimental data an over-prediction of drag is observed. This is attributed to the use of wall functions interfering with the modelling of shear layers.[37] For flows over a curved surface such as an airfoil, this requires capturing of near wall features such as a resolved boundary layer and any reversed flows due to adverse pressure gradients. However, for the context of wake studies, capturing the boundary layer may be of less significance. This is where hybrid methods like DES prevails. As vortex shedding involves the physical detachment of flow from the body, the modelling of the shedding of turbulent structures from the boundary layer or near wall region and transition into wake would have to be considered. This encourages further studies on the impact of DES and its RANS-modelled wall regions against full LES methods on downstream wakes. This is important in the context of modelling of aerodynamic interactions. It would be useful to advance the understanding and implications of applying DES and as compared to LES models for the purposes wake studies.

Conceptually, the wing in such a context is a vortex generator. Therefore, for further extending this study into one which provides insight on the effectiveness of a horizontal stabilizer within a turbulent wake, the wings in this case may be replaced by an upstream vortex generator of a much simplified geometry. This is analogous to studies conducted on the assessment of aerodynamic bodies within turbulence.

Acknowledgments

References

[1]B. Etkin, Dynamics of Atmospheric Flight, Dover Publications, 1972.

[2]B. Etkin and L. D. Reid, "Chapter 2: Static Stability and Control - Part I," in Dynamics of Flight, Wiley, 1994, pp. 18-33.

[3]R. C. Nelson, "2.3 Static Stability and Control," in Flight Stability and Automatic Control, WCB/McGraw-Hill, 1998, pp. 47-52.

[4]W. F. Philips, "Chapter 4: Longitudinal Static Stability and Trim," in Mechanics of Flight, Wiley, 2010, pp. 384-391.

[5]K. J. B. Tan and P. C. Wang, "Computational Modelling and Aerodynamic Analysis of a Conventional Fixed-Wing Aircraft," in Advances in Simulation: The Future of Flight Simulation, London, 2016.

[6]"Aerodynamic Data for Structural Loads: C-130," Lockheed, California, 1953.

[7]J. J. D. Anderson, "Chapter 5: Incompressible Flow over Finite Wings," in Fundamentals of Aerdynamics, New York, McGraw-Hill, 2001, pp. 412-484.

[8]A. Silverstein and S. Katzopf, "Design Charts for Predicting Downwash Angles and Wake Characteristics Behind Plain and Flapped Wings," NACA, 1939.

[9]A. Silverstein, S. Katzopf and W. K. Bullivant, "Downwash and Wake Behind Plain and Flapped Airfoils," NACA, 1939.

[10]J. D. Anderson, Jr., "Chapter 2: Aerodynamics of the Airplane: The Drag Polar," in Aircraft Performance and Design, McGraw-Hill Book Co.-Singapore, 1999, pp. 103-105.

[11]C. Paek, J. Chung and R. Czerwiec, "C-130 Aerodynamic Loads Assessment for the USN/USMC Part I: P-3C CFD Verification," in 47th AIAA Aerospace Sciences Meeting Including The New Horizons Forum and Aerospace Exposition, Orlando, Florida, 2009.

[12]J. Chung, C. Paek and R. Czerwiec, "C-130 Aerodynamic Loads Assessment for the USN/USMC Part II: C-130 Analysis," in 47th AIAA Aerospace Sciences Meeting Including The New Horizons Forum and Aerospace Exposition, Orlando, Florida, 2009.

[13]M. Ghoreyshi and R. M. Cummings, "From Spreadsheets to Simulation-Based Aircraft Conceptual Design," Applied Physics Research, vol. 6, no. 3, 2014.

[14]F. H. Proctor, "Numerical Simulation of Wake Vortices Measured During the Idaho Falls and Memphis Field Programs," in 14th AIAA Applied Aerodynamic Conference, New Orleans, Louisiana, 1996.

[15]D. P. Delisi, G. C. Greene, R. E. Robins, D. C. Vicroy and F. Y. Wang, "Aircraft Wake Vortex Core Size Measurements," in 21st AIAA Applied Aerodynamics Conference, Orlando, FL, 2003.

[16]N. N. Ahmad, F. H. Proctor, F. M. L. Duparcmeur and D. Jacob, "Review of Idealized Aircraft Wake Vortex Models," in AIAA SciTech, National Harbor, Maryland, 2014.

[17]F. T. Johnson and E. N. Tinoco, "Thirty Years of Development and Application of CFD at Boeing Commercial Airplanes, Seattle, Washington," American Institute of Aeronautics and Astronautics, 2005.

[18]M. R. Hall, R. T. Biedron, D. N. Ball, D. R. Bogue, J. Chung, B. E. Green, M. J. Grismer, G. P. Brooks and J. R. Chambers, "Computational Methods for Stability and Control (COMSAC): The Time Has Come," American Institute of Aeronautics and Astronautics, 2004.

[19]S. A. Morton, J. R. Forsythe, K. D. Squires and R. M. Cummings, "Detached-Eddy Simulations of Full Aircraft Experiencing Massively Separated Flows," in The 5th Asian Computational Fluid Dynamics Conference, Busan, Korea, 2003.

[20]D. Drikakis, D. Kwak and C. C. Kiris, "Computational Aerodynamics: Advances and Challenges," The Aeronautical Journal, vol. 120, no. 1223, pp. 13-36, 2016.

[21]P. R. Spalart and V. Venkatakrishnan, "On the Role and Challenges of CFD in the Aerospace Industry," The Aeronautical Journal, vol. 120, no. 1223, pp. 209-231, 2016.

[22]P. R. Spalart, W.-H. Jou, M. Strelets and S. R. Allmaras, "Comments on the Feasibility of LES for Wings, and on a Hybrid RANS/LES Approach," in Advances in DNS/LES, 1997.

[23]P. R. Spalart, S. Deck, M. L. Shur, K. D. Squires, M. K. Strelets and A. Travin, "A New Version of Detached-Eddy Simulation, Resistant to Ambiguous Grid Densities," Theoretical and Computational Fluid Dynamics, pp. 181-195, 2006.

[24]P. R. Spalart, "Young-Person's Guide to Detached-Eddy Simulation Grids," NASA Langley Research Center, Virginia, 2001.

[25]J. R. Forsythe, K. D. Squires, K. E. Wurtzler and P. R. Spalart, "Detached-Eddy Simulation of the F-15E at High Alpha," Journal of Aircraft, vol. 41, no. 2, 2004.

[26]Customer Training Systems Department, "Volume I: General Aircraft," in C-130H-30 Hercules Traning Manual, Lockheed Aeronautical Systems Company - Georgia, 1993, pp. 2-5.

[27]P. R. Spalart and S. R. Allmaras, "A One-Equation Turbulence Model for Aerodynamic Flows," in AIAA 30th Aerospace Sciences Meeting and Exhibit, Reno, NV, 1993.

[28]C. L. Rumsey, "Apparent Transition Behavior of Widely-Used Turbulence Models," Apparent Transition Behavior of Widely-Used Turbulence Models, vol. 28, pp. 1460-1471, 2007.

[29]C. L. Rumsey, D. O. Allison, R. T. Biedron, P. G. Buning, T. G. Gainer, J. H. Morrison, S. M. Rivers, S. J. Mysko and D. P. Witkowski, "CFD Sensitivity Analysis of a Modern Civil Transport Near Buffet-Onset Conditons," NASA/TM-2001-211263, 2001.

[30]NASA Langley Research Center, "Turbulence Modeling Resource," NASA, 2016. [Online]. Available: https://turbmodels.larc.nasa.gov/spalart.html. [Accessed March 2017].

[31]J. H. Ferziger and P. M., Computational Methods for Fluid Dynamics, Springer-Verlag, 2001.

[32]C. M. Fremaux and R. . M. Hall, "(Compilation) COMSAC: Computational Methods for Stability and Control," Virginia, 2004.

[33]P. C. Wang, "Large Eddy Simulation of High Speed Convergent-Divergent Nozzle Flows, PhD Thesis," Loughborough University, 2012.

[34]H. Schlichting, Boundary Layer Theory, McGraw-Hill Science/Engineering/Math, 1979.

[35]R. Courant, K. Friedrichs and H. Lewy, "On the Partial Difference Equations of Mathematical Physics," AEC Research and Development Report, NYO-7689, New York: AEC Computing and Applied Mathematics Centre, New York, 2008.

[36]F. Holzapfel, "Aircraft Wake Vortex Evolotuion and Prediction," 2005.

[37]J. D. Anderson, Jr., "Chapter 4: Incompressible Flow Over Airfoils," in Fundamentals of Aerodynamics, New York, McGraw-Hill, 2011, pp. 334-338.

[38]E. N. Tinoco, O. P. Brodersen, S. Keye, K. R. Laflin, E. Feltrop, J. C. Vassberg, M. Mani, B. Rider, R. A. Wahls, J. H. Morrison, D. Hue, M. Gariepy, C. J. Roy, D. J. Mavriplis and M. Murayama, "Summary of Data from the Sixth AIAA CFD Drag Prediction Workshop: CRM Cases 2 to 5," in Drag Prediction Workshop, 2016.